

pubs.acs.org/acsapm Article

Systematic Modulation and Structure—Property Relationships in Photopolymerizable Thermoplastics

Kimberly K. Childress, Marvin D. Alim, Sudheendran Mavila, Vikina Martinez, Yifu Ding, Christopher N. Bowman, and Jeffrey W. Stansbury*



Cite This: ACS Appl. Polym. Mater. 2021, 3, 1171-1181



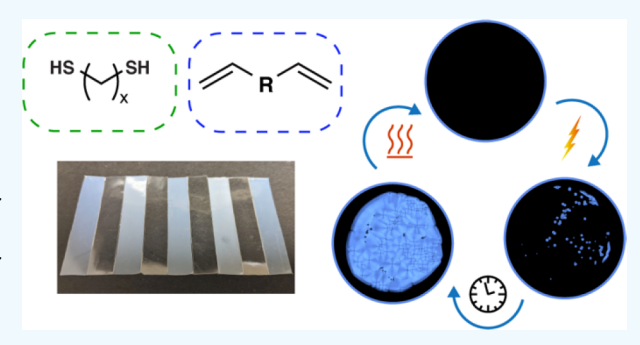
ACCESS

Metrics & More



s Supporting Information

ABSTRACT: Thermoplastics encompass the majority of commercial plastics but are limited to manufacturing techniques that require heat and/or solvent to enable material reprocessing and reshaping. Photopolymerization offers a readily accessible in situ alternative to conventional processing techniques but has typically been restricted to cross-linked networks, thus removing the potential for recycling/reprocessing of the materials. In this work, the paradigm of photopolymerizable thermoplastics consisting of semicrystalline thiol—ene polymers with repeat units structures mimicking those of poly(ethylene terephthalate) is explored. These materials are rapidly photopolymerized (<10 s) under mild irradiation conditions by using commercially available, unpurified dithiol and diene monomers to give



polymeric materials with distinctive mechanical properties. The complex relationships between monomer structure, crystallization, and material properties (optical, thermal, and mechanical) were investigated by modifying the dithiol alkyl chain length (xDT, x = 2-10). Though subtle, these monomeric structural perturbations significantly impacted both the rate ($\sim 0.3-19$ MPa min⁻¹) and extent of crystallization as well as the corresponding material properties (e.g., Young's modulus and elongation to break ranging from 80-280 MPa and 500-840%, respectively). To confirm the expansive applicability of this facile photopolymerization method, substitutions to the diene functionalities that participate in crystallization were explored to understand the relationship between the monomer structure, the extent of crystallinity, and the mechanical performance. The photopolymers reported herein provide a basic framework to expand access to photocurable step-growth linear polymers with well-controlled polymerization-induced crystallization for a variety of applications, including for the rapid manufacture of prototypical or sacrificial components in 3D printing.

KEYWORDS: polymerization-induced crystallization, thiol—ene, photopolymerization, polymer structure—properties, toughness, thermoplastic

■ INTRODUCTION

Thermoplastics ranging from amorphous (polystyrene, acrylics, polycarbonate, acrylonitrile-butadiene-styrene, and poly-(vinyl chloride)) to semicrystalline (polyethylene, polypropylene, polyamides, poly(ethylene terephthalate), and polyether ether ketone) constitute the majority of plastics produced for commercial use. Their pliability at elevated temperatures enables the rapid manufacture of predetermined components, achieving a wide array of desirable material properties (e.g., thermal resistance, transparency, and mechanical strength). Such properties are governed by the amorphous structure in terms of glass transition temperature (T_{σ}) and chain entanglements, whereas semicrystalline polymer behavior is also directed by the morphology and extent of the crystalline domains. Additionally, whereas thermosets have a permanent cross-linked structure, thermoplastics are moldable upon heating, facilitating recycling and secondary processing. However, the applicability of thermoplastics formed by conventional methods (injection molding and extrusion) is limited to specific processing conditions and a select number of materials. Uniquely, photopolymerizations offer a facile and economical approach to expand the range of functionally useful materials and parts by offering spatiotemporal control of the polymerization and relatively rapid reaction kinetics even at ambient conditions. Such advantages have fostered its utility in a growing number of industrial applications, including coatings, adhesives, dental materials, and 3D printing, to name a few.

Photopolymerizable thermoplastics expand the applicable scope of polymeric materials. However, the vast majority of functional photopolymers are formulated with some degree of

Received: December 20, 2020 Accepted: January 19, 2021 Published: January 21, 2021





cross-linking, inhibiting or eliminating potential reprocessability. In this respect, the expanding field of covalent adaptable networks (CANs) broadly seeks to bridge the divide between thermosets and thermoplastics through the inclusion of dynamic covalent chemistries into covalently cross-linked networks.^{2–4} While dissociative dynamic networks enable flow in a manner similar to thermoplastics, the utility of these different CANs is limited to particular functionalities and often requires cumbersome external stimuli, custom chemistries, or specific catalysts. For this reason, it is advantageous to simultaneously consider the development of thermoplastic systems that both possess properties comparable to thermosets and are readily reprocessable with heat or solvent. (Meth)acrylates initially appeared to be promising thermoplastic candidates due to their readily available monomers with significant structure-property variations. However, the desirable properties realized in photopolymerizable thermosets do not translate to thermoplastics as slow polymerization rates, low molecular weights, and brittle final materials are often observed for linear or mostly linear (meth)acrylate systems. For these reasons, there are relatively few reports on photopolymers made with monofunctional (meth)acrylates. One such example implemented acryloylmorpholines, which undergo chain-growth photopolymerization similar to (meth)acrylates, to rapidly 3D print complex sacrificial structures for functional use.⁵ This work facilitated many technological opportunities but was limited in use and required materials with T_g higher than the printing temperature.

In contrast to these traditional chain-growth photopolymers, thiol-ene "click" chemistry offers a promising substitute to conventional (meth)acrylates as it bypasses several fundamental limitations, including oxygen inhibition,6 stress relaxation,7 and heterogeneous network formation. Initially used to photopolymerize dithiols and dienes in 1948,8 thiol-enes are promising candidates for achieving high molecular weight materials. Recently, the stringent reaction conditions necessary for step-growth polymerizations were effectuated for thiol-ene miniemulsion, postmodification of branched polymethacrylates, 10 and generation of sequence-specific functional polymers with high molecular weights.11-18 While considerable work has been done to construct specialized materials with thiol-ene reactions, comparably little effort has been dedicated to the development of photopolymerizable materials that mirror the properties available in industrial thermoplastics. Jin et al. achieved high molecular weight photopolymers ($\sim 10^4$ g mol⁻¹) with good mechanical properties via thiolnorbornene reactions but obtained comparably low molecular weights (~103 g mol-1) and a poor mechanical response for thiol-vinyl systems. 19 Recently, our group demonstrated a facile, high molecular weight thiol-ene photopolymer material structurally mimicking poly(ethylene terephthalate) and possessing excellent mechanical properties with high ductility and toughness.²⁰ The substantial robustness manifested for these semicrystalline photopolymers facilitated its implementation for 3D printing, and the thermal manipulation of printed structures was further validated at relatively low temperatures (90 °C), making them good candidates for recycling or reuse.

These promising results motivated a more expansive investigation into the structure—property relationships and material properties (i.e., optical, thermal, and mechanical) of related photopolymerizable thiol—ene systems. To simplify the structure—property analysis and perform a more thorough investigation, incremental structural changes to the dithiol

monomer were applied by varying the length of the flexible alkyl chain. In doing so, a closer examination into the relationship between monomer structure, crystallization, and material properties was achieved. Furthermore, an investigation into diene substitutions was supplemented to simultaneously probe the dependence of crystallization on various monomer functionalities and demonstrate the versatility of this photopolymerization technique. We hope this work provides a foundation for expanding the material property space for practical photopolymerizable thermoplastics.

■ EXPERIMENTAL SECTION

Materials. Diphenyl-(2,4,6-trimethylbenzoyl)phosphine oxide (TPO, listed purity: >98%), diallyl terephthalate (DAT, ≥98%), 1,4-butanedithiol (4DT, >95%), 1,10-decanedithiol (10DT, >98%), divinyl adipate (DVA, 96%), diallyl adipate (DAA, 98%), diallyl isophthalate (DAI, 98%), and 3,9-divinylspirobi(*m*-dioxane) (DVSD, 98%) were purchased from TCI America. 1,2-Ethanedithiol (EDT, ≥98%), 1,6-hexanedithiol (6DT, ≥98%), and diallyl carbonate (DAC, 99%) were purchased from MilliporeSigma. 1,3-Propanedithiol (3DT, 97%), 1,5-pentanedithiol (5DT, 96%), 1,8-octanedithiol (8DT, 98%), and 1,9-nonanedithiol (9DT, 97%) were purchased from Alfa Aesar. Bisphenol A diallyl ether (Matrimid 2292, BADE, 89−93%) was purchased from Huntsman. All chemicals were used as received without further purification.

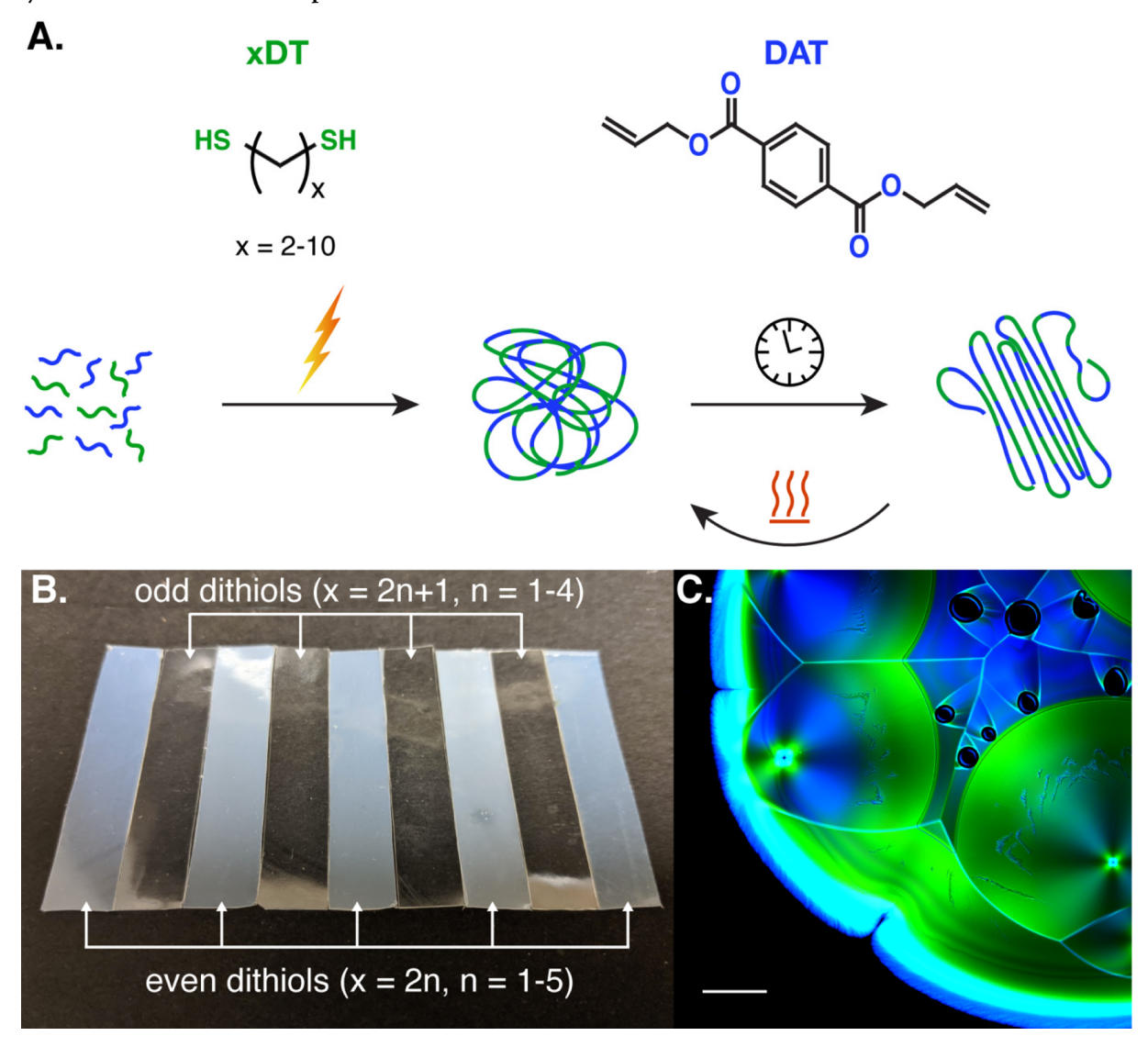
Methods. Synthesis of 1,4-Bis(allyloxy)benzene (DAQ). To a 250 mL round-bottomed flask equipped with a reflux condenser and stir

bar was added 5.0 g (45.4 mmol, 1 equiv) of *p*-dihydroxybenzene and was dissolved in 90 mL of CH₃CN. To this was added 15.7 g (113.5 mmol, 2.5 equiv) of K_2CO_3 followed by 9.8 mL (13.7 g, 113.5 mmol, 2.5 equiv) of allyl bromide under a N_2 atmosphere. The resulting reaction mixture was refluxed for 16 h. After this period, the flask was cooled to room temperature, the solid was filtered off, and the filtrate was evaporated under reduced pressure to yield the crude product which was purified by silica-gel column chromatography eluting with 5% EtOAc/hexanes. Evaporation of the fraction containing the product under reduced pressure yielded 6.2 g (72%) of the title compound as white solid which was used for the subsequent studies with no further purifications. ¹H NMR (400 MHz, chloroform-d): δ 6.85 (m, 2H), δ .10– δ .00 (m, 2H), δ .42– δ .26 (m, 4H), 4.48 (dt, δ = 5.3, 1.5 Hz, 4H). ¹³C NMR (101 MHz, chloroform- δ): δ 153.0, 133.7, 117.6, 115.8, 69.6.

Synthesis of 1,7-Heptanedithiol (7DT). To a 250 mL round-bottomed flask equipped with a reflux condenser and stir bar was

added 3.3 mL (5.0 g, 19.4 mmol, 1 equiv) of 1,7-dibromoheptane and was dissolved in 65 mL of 95% ethanol. To this solution, 2.9 g (38.7 mmol, 2 equiv) of thiourea was added and heated to reflux for 55 h under a N_2 atmosphere. After this period, the flask was cooled to room temperature, and the solvent was evaporated under reduced pressure to give the thiouronium salt as white solid. To this, a solution of 1.55 g (38.7 mmol, 2 equiv) of sodium hydroxide dissolved 65 mL of deionized water was added, and the resulting suspension was then allowed to reflux for 1 h. After this period, the flask was cooled to room temperature, acidified to pH \approx 1–2 with 1 N hydrochloric acid solution, and extracted with CH₂Cl₂ (5 × 50 mL). The combined organic extracts were washed with water (\sim 50 mL, 1×) and brine (50 mL, 1×), dried over Na_2SO_4 , filtered, and evaporated under reduced

Scheme 1. (A) Overview of Thermoplastic Photopolymerization and Reprocessing; a (B) Apparent Optical Discrepancies for Freestanding XDT-DAT Films Are Observed and Presented in Order of Increasing Alkyl Chain Length; b (C) POM Image of a Semicrystalline Thiol—Ene Thermoplastic c



"Liquid monomers xDT (where x = the number of carbons in the alkyl chain) and DAT undergo rapid, light-induced polymerization to yield polymers with high molecular weights. Over a subsequent period of time, the amorphous polymers undergo long-range molecular ordering and become semicrystalline. The non-cross-linked polymer chains can then achieve pliability upon heating for secondary use. ^bFrom left to right, x = 2, x = 3, ... x = 10). ^c3DT-DAT shown here; scale bar: 50 μ m.

pressure to give the crude product which was purified by silica-gel column chromatography eluting with 10% EtOAc/hexanes. Evaporation of the fraction containing the product under reduced pressure yielded 2.5 g (78%) of the title compound as a colorless oil which was used for the subsequent studies with no further purifications. $^1\mathrm{H}$ NMR (400 MHz, chloroform-d): δ 2.60–2.45 (m, 4H), 1.68–1.52 (m, 4H), 1.46–1.23 (m, 8H), 1.33 (t, J=7.8 Hz, 3H). $^{13}\mathrm{C}$ NMR (101 MHz, chloroform-d): δ 34.0, 28.6, 28.3, 24.7.

Bulk Film Preparation. 1 mol % photoinitiator TPO (with respect to the thiol functional group) was well mixed with a stoichiometric solution of dithiol and diene monomers in a 20 mL scintillation vial. Films were then cast on large glass plates with 250 μ m plastic shims to control thickness and fixed with large binder clips to hold the glass plates together. The thiol—ene solution was then irradiated on each side for 5 min with a 405 nm LED source (ECO UV bar) at ~7 mW cm⁻².

Fourier Transform Infrared Spectroscopy (FTIR). FTIR was used to determine thiol-ene polymerization kinetics by integrating the

representative thiol (2550–2600 cm⁻¹) and carbon–carbon double bond (1650–1680 cm⁻¹) peaks in real time by using a series scan. A Thermo Scientific Nicolet 6700 FTIR spectrometer was coupled to a myDAQ (National Instruments) to synchronize monomer irradiation with a collimated 405 nm LED (1 mW cm⁻¹, Thorlabs, Inc.) and data acquisition with the software. Optically thin samples with 15 $\mu \rm m$ spacers were prepared between salt (NaCl) plates. By monitoring peak integration in real time, the thiol conversion ($c_{\rm thiol}$) and vinyl conversion ($c_{\rm vinyl}$) were calculated by

$$C = \left(1 - \frac{A}{A_{\text{initial}}}\right) \tag{1}$$

where $A_{\rm initial}$ is peak area of the thiol or C=C functional group prior to irradiation and A is peak area at a given time during polymerization. Real-Time Photorheology. A rotational rheometer (ARES-G2, TA Instruments) equipped with a parallel plate geometry was used to investigate thiol—ene crystallization through modulus development in

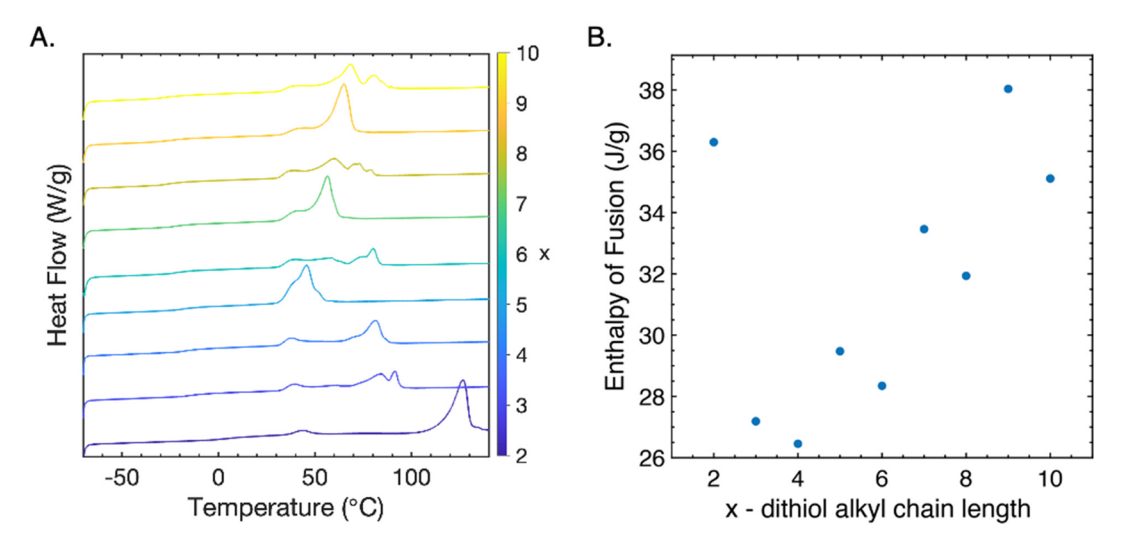


Figure 1. Thermal transitions of xDT-DAT photopolymers. (A) Initial heating ramp with DSC revealed clear melting endotherms for the thermoplastic systems (endo up). Variations in melting temperatures were observed with monomer selection. (B) Enthalpy of fusion generally increased with increasing alkyl chain length (with the exception of 2DT-DAT) due to increased chain flexibility.

real time. Using a UV-transmissible 20 mm diameter quartz plate and mirrors, we monitored the storage modulus (G'), loss modulus (G''), and complex viscosity (η^*) after irradiation with a collimated 405 nm LED (Thorlabs, Inc.) at 25 mW cm⁻² for 30 s. The monomer was isothermally equilibrated at 25 °C for 60 s prior to irradiation. The oscillation fast procedure was used for a gap thickness of 0.2 mm (70 μ L of monomer) with a sampling rate of 4 pts/s, a strain of 2%, and a frequency of 10 Hz for a total of 3600 s.

Polarized Optical Microscopy (POM). High resolution and temporal imaging were performed by using a Nikon Ti-E microscope. Crystallization videos were obtained by using a 20× 0.75 NA objective upon irradiation with an Excelitas Xcite 120 light source and a 360/40 nm excitation band-pass filter. Monomer was irradiated at \sim 50 mW cm⁻² for 1 s, and 4 × 4 images were obtained postirradiation for several minutes. Images were subsequently acquired of the polymerized area. Images and videos were processed with Nikon Elements software (ver. 4.5).

Differential Scanning Calorimetry (DSC). Thermal transitions were monitored with a DSC2500 (TA Instruments). 6-7 mg of material was loaded into hermetically sealed aluminum pans (TA Instruments). To be consistent with the crystallinity conditions of samples used for thermal and mechanical testing, the degree of crystallinity was approximated from materials used "as received"; i.e., thermal history was not removed via an initial heating cycle. The relative degrees of crystallinity between the thiol-ene samples was determined by integrating the heating exotherm (-70 to 150 °C at a heating rate of 10 °C/min). The crystallization temperature (T_c) and melting temperature (T_m) for each thiol-ene material were obtained by heating a sample under nitrogen from -70 °C to \sim 40 °C above its maximum T_m at 10 °C/min and isothermally holding for 20 min to remove thermal history. The samples were then cooled at 10 °C/min to $-70~^{\circ}\text{C}$ and isothermally held for 15 min before reheating at 10 $^{\circ}$ C/min to \sim 20 $^{\circ}$ C above its maximum T_{m} .

Wide-Angle X-ray Scattering (WAXS). WAXS patterns were obtained for each thiol-ene material at room temperature (~20 $^{\circ}\text{C})$ with a 30 W Genix 3D X-ray generator (Cu anode, λ = 0.154 nm) and a Dectris Eiger R 1M detector. The operating target voltage and tube current were 50 keV and 0.6 mA, respectively. The scanning speed was 1 h/frame.

Dynamic Mechanical Analysis (DMA). DMA was performed to obtain tan δ and storage modulus as a function of temperature by using an RSA-G2 Solids Analyzer (TA Instruments). Rectangular films were heated at 3 °C/min, and a frequency of 1 Hz and a fixed strain of 0.1% were applied after equilibrating at −70 °C. Heating was applied twice to remove thermal history from the first run.

Size-Exclusion Chromatography with Multiangle Light Scattering (SEC-MALS). A size-exclusion chromatography instrument (Tosoh EcoSEC) equipped with a UV and differential refractive index detector (100 μ L injection volume) was used in combination with a multiangle light scattering detector (Wyatt Treos II) for thiol-ene samples soluble in THF. THF was used as the eluent at a flow rate of 1 mL/min

Mechanical Tensile Testing. Uniaxial tensile tests (Exceed Model E42, 500 N load cell, MTS Systems Corporation) were performed on dog bones cut from bulk films (ASTM D638 Type V) with thicknesses of \sim 250 μ m. The dog bones were strained at 5 mm/ min at ambient temperature. Young's modulus (E) was calculated by using the 1-2% strain region on the linear elastic regime of the stress-strain curve, and toughness (T) was calculated as the area under the stress-strain curve.

Ultraviolet-Visible (UV-Vis) Optical Transmittance. Optical transmittance was measured through 25 µm thick xDT-DAT films from 300 to 800 nm on an Evolution 300 UV-vis (Thermo Scientific) at a scanning speed of 60 nm min⁻¹.

RESULTS

Fundamental structure-property relationships of photopolymerizable thermoplastics were established through systematic variation of the dithiol alkyl chain length in stoichiometric thiol-ene photopolymer formulations with diallyl terephthalate (DAT) to form xDT-DAT (x = 2-10) photopolymers. Arranging the bulk xDT-DAT photopolymer films side-by-side (Scheme 1), a striking odd-even trend in relative opacity was observed. Odd samples (x = 2n + 1, n = 1-4) appeared optically transparent/translucent whereas the even samples (x= 2n, n = 1-5) were opaque. While all photopolymerized films (near-quantitative conversions separately confirmed with FTIR, Figure S1) were initially transparent, the odd samples only became translucent over a settling period. Conversely, the initially transparent even samples converged to a high degree of opacity over a period of seconds or minutes. These definitive differences in optical behavior at equilibrium were verified by UV-vis transmittance measurements (Figure S2).

While the eventual optical transition from transparent to opaque has previously been reported and attributed to the crystallization of polymeric chains, 20,21 the transparent/translucent appearance of the odd samples did not automatically preclude minimal to no crystallization as many commercial semicrystalline yet essentially clear polymers exist, such as poly(ethylene terephthalate) and poly(ethylene naphthalate). Therefore, to reliably detect the absence or presence of crystallinity, differential scanning calorimetry (DSC) was used to detect first-order thermal transitions. Using standard heat cool-heat cycles, we clearly observed melting endothermic transitions upon heating for all xDT-DAT samples (Figure 1A). However, closer examination of the individual DSC traces revealed different melting endotherm profiles between odd and even samples. With the exception of 2DT-DAT, the even samples characteristically had broad profiles with multiple peaks, which is typically indicative of nonuniform crystallite formation and is a common occurrence in semicrystalline thermoplastics. ^{21–27} In contrast, the odd thiol—ene samples exhibited only a single, dominant endotherm with a small but distinctive shoulder at lower temperatures (with the exception of 3DT-DAT). Stable crystals with thicker lamella formed during primary crystallization require more thermal energy to melt and thus exhibit higher melting temperatures (T_m) . Conversely, smaller, imperfect crystals with thinner lamella develop at longer times during secondary crystallization and require less energy to achieve the melt state. Thus, the DSC results suggest that crystals in the odd samples developed more uniform lamella than the even samples.

While a direct comparison of the melting temperatures of the xDT-DAT samples was complicated due to the multimodal endothermic peaks of the even samples, an examination of the global maximum temperature $(T_{m,max})$ of the endotherm for each system revealed a clear odd-even effect. Odd samples had a considerably lower $T_{m,max}$ than the even samples, which can be explained by the packing efficiency of the alkyl chains. Alkyl chains with an even number of carbons exhibit a planar zigzag configuration that facilitates optimal chain packing. Conversely, the nonplanar structure of the odd-carboncontaining alkyl chains causes the zigzag conformation to orient slightly out of plane, generating significant torsional strain and disrupting long-range crystalline ordering.²⁸⁻³¹ These apparent odd-even effects were observed for samples with x = 4-10, whereas peculiar thermal transitions were observed when x = 2-3. Longer aliphatic chains favor an alltrans conformation, and therefore crystalline packing is only dependent on alkyl chain planarity. On the other hand, shorter alkyl chains possess gauche bonds of opposite sense that separate the trans bonds. The ensuant kinked conformation acts to stabilize the crystals by encouraging good intermolecular packing with a modest intramolecular energy penalty, ultimately increasing $T_{\rm m}$.

The melting temperature showed a strong dependence on alkyl chain planarity and conformation, whereas the enthalpy of fusion (with the exception of 2DT-DAT) increased with increasing chain length. Similar relationships between crystallinity and chain length were previously observed and can be attributed to an increase in chain flexibility that facilitates better chain packing into the crystalline domains, thus achieving a higher degree of crystallinity. $^{13,33-35}$ While absolute degrees of crystallinity cannot be determined from DSC because the enthalpy of the purely crystalline material is unknown, relative crystallinity trends can be determined because of their structural similarity of the materials. 13 Likewise, dynamic mechanical analysis (DMA) revealed that $T_{\rm g}$ was solely dependent on the mobility of the alkyl chains where longer chains had lower $T_{\rm g}$ values (Figure S3). 28,29,36,37

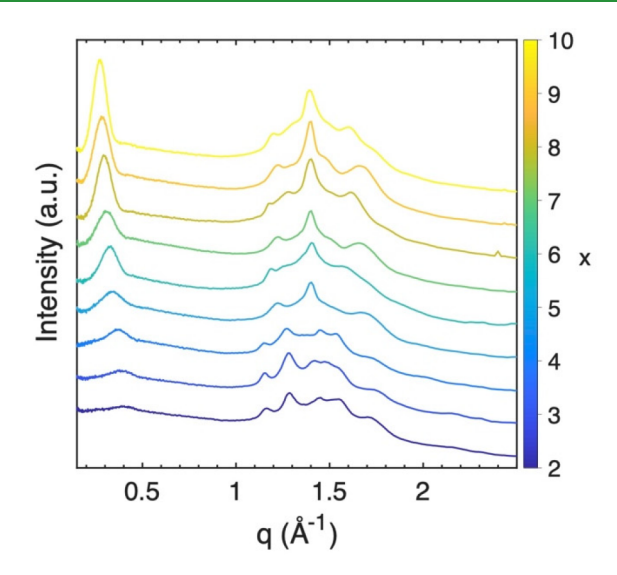


Figure 2. 1D WAXS intensity profiles for the xDT-DAT thiol—ene thermoplastics, wherex is the carbon spacer length of the dithiol. WAXS revealed a clear homogenization of the crystalline structure with increasing alkyl chain length.

The crystallinity of the xDT-DAT samples was further characterized with wide-angle X-ray scattering (WAXS). Because these materials were photopolymerized under ambient conditions without strictly controlling the crystallization conditions, the samples were polymorphic as revealed by their multiple peaks. 13 Blunted diffraction patterns with several shallow peaks were observed for xDT-DAT samples with shorter alkyl chains (x = 2-4) and have likewise been observed for linear polymers with short aliphatic chains. 33,35 Conversely, fewer and narrower peaks with higher intensities were observed for samples with longer alkyl chains (x = 5-10) because of the homogenization of the crystalline structures and the formation of larger crystallites. This difference in crystallinity is attributed to both differences in chain conformation, where the shorter chains will possess a higher degree of gauche bonds, and the higher concentration of ester groups present in the shorter chains, which act as lattice defects.

Subtle variances in alkyl chain length yielded pronounced differences in polymer crystallinity that influenced thermal and optical properties. To determine whether the rates of crystallization were likewise affected, the storage (G') and loss (G") moduli were monitored in real time via photorheology (Figure 3A). Consistent with the rapid polymerization rates observed via real-time FTIR, 405 nm irradiation resulted in a rapid increase and subsequent crossover of G' and G'', signifying the transition from a liquid-like to a solid-like material.³⁸ Crystallization concomitant with polymerization resulted in a second modulus increase, followed by a plateau in G' and a drop in G'' below the detection limits of the rheometer. 20 Because polymerization and crystallization overlap (to varying degrees), it is difficult to isolate rates of crystallization. However, the rates of polymerization for all of the xDT-DAT samples were nearly identical and presumably do not contribute to the large differences observed during the secondary modulus development (Figure S4). Therefore, crystallization rates were approximated by observing the rate of change in G' from the start of irradiation to the onset of the G' plateau (termination of crystallization) (Figure 3B). Interestingly, with the exception of 2DT, a pseudo-sigmoidal

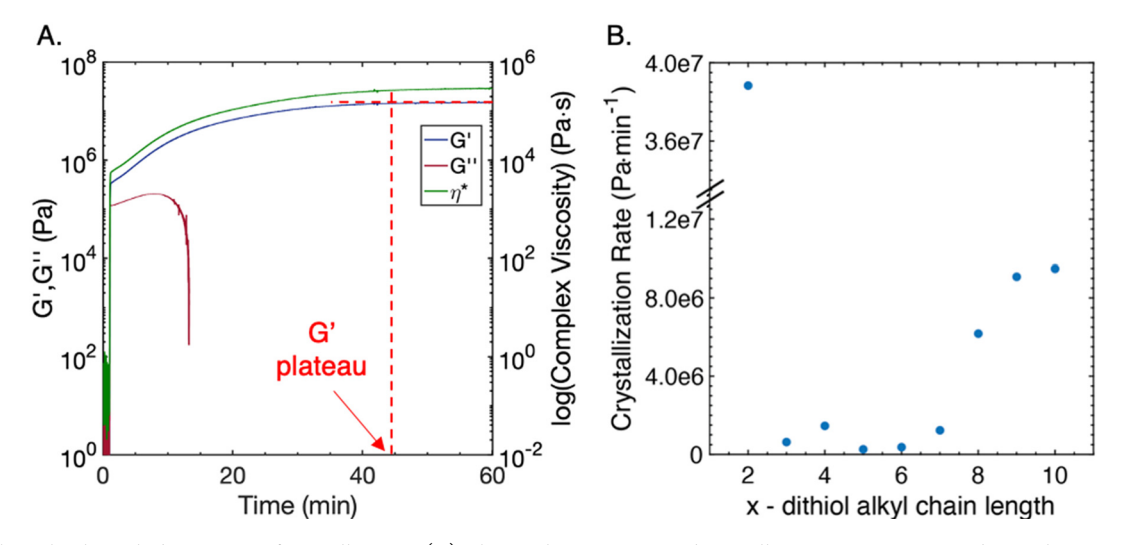


Figure 3. Photorheological observation of crystallization. (A) Photopolymerization and crystallization were monitored in real time via G' and G'' moduli development (6DT-DAT shown here). A sharp modulus increase was initially observed due to photopolymerization (405 nm LED, 25 mW cm⁻²). A concurrent secondary G' increase was observed due to crystallization along with a drop in G'' below the detection limits of the instrument and a concomitant rise in η^* . (B) Onset of the G' plateau was approximated as the termination of crystallization for each thiol—ene sample, and a faster rate of crystallization was observed for samples with longer dithiol chains (with the exception of 2DT).

crystallization profile was evident with the longer alkyl chain samples exhibiting the fastest rates of crystallization. High rates of crystallization were also observed for 2DT-DAT, likely because of its large degree of supercooling $(T_{\rm m} - T_{\rm c})$ where $T_{\rm c}$ is the crystallization temperature) relative to the other thermoplastics as well as the increased crystalline stabilization of its kinked chain. This study shows that slight modifications in monomer structure remarkably alter the range of attainable crystallization times. While the final material properties are generally used to determine material suitability for a given applications, the crystallization rate also has significant implications on its processability and industrial utility. For example, fast crystallization kinetics are advantageous for applications that entail melt processing as crystallinity limits distortion upon removal from the mold and reduces cycle times.³⁹ Conversely, slower crystallization rates may be beneficial for applications whereby rapid crystallization would inhibit adhesion and impact material homogeneity (e.g., layerby-layer 3D printing). For any of these materials, further control of the tunable range of the crystallization rate may also be obtained via techniques such as the addition of nucleating agents 40-42 or by controlling the processing temperature. 43

Aside from the discussed aspects of crystallinity in polymers, their mechanical performance strongly influences their utility. As the linear polymer's molecular weight significantly affects their mechanical properties,44 the molecular weight and polydispersity of xDT-DAT samples were measured by using size-exclusion chromatography with multiangle light scattering (SEC-MALS) in tetrahydrofuran (THF). Similar to poly-(ethylene terephthalate) (PET), samples of shorter alkyl chain lengths (x = 2-5) were insoluble in THF and other common solvents at elevated temperatures. 45 Of the THF-soluble xDT-DAT samples (x = 6-10), all samples exhibited numberaverage molecular weights (M_n) on the order of 10^4 g mol⁻¹ with polydispersity values around 2 (Table 1) even though the thiol-ene stoichiometry was approximated with unpurified monomers (with the exception of the synthesized 1,7heptanedithiol). Step-growth theory dictates that high molecular weights are achieved through the polymerization

Table 1. SEC-MALS Eluted in THF Was Used to Obtain M_n and PDI for xDT-DAT Thiol—Ene Samples for $x > 5^a$

\boldsymbol{x}	$M_{\rm n}~({ m g~mol^{-1}})$	PDI
6	6×10^{4}	2.6
7	4×10^{4}	2.0
8	4×10^{4}	1.8
9	3×10^4	2.0
10	3×10^4	1.7

^aSamples with shorter alkyl chains were not soluble in THF.

of a stoichiometric mixture of pure monomers to high degrees of conversion. Indeed, it is unlikely that the systems studied here fully meet those criteria. Thus, we suspect that even higher molecular weights are possible through the more careful control of initial polymerization conditions. In the case of the residual monomers present in the systems studied, we hypothesize that they may limit the crystallization process by acting as plasticizers.

Mechanical testing of all xDT-DAT samples was performed with uniaxial tensile tests on 150 μ m thick ASTM D638 Type V dog bones. As seen by the representative stress-strain plot (Figure 4A), the characteristic semicrystalline deformation behavior⁴⁶ of all xDT-DAT samples in tension exhibited a modest elastic deformation and yielding followed by a pronounced degree of strain softening and strain hardening, resulting in appreciably high elongations to break (ϵ_{\max}) of up to 840%. Whereas this plasticity is simply attributed to high molecular weights and significant degrees of chain entanglements in amorphous materials, the deformation behavior of semicrystalline polymers is complex due to the intricate molecular interplay between the degree of polymerization (and thus the extent of chain entanglements) and the crystalline microstructure. While assigning mechanical properties to specific polymers is impractical, some dependencies on alkyl dithiol length or planarity for select mechanical properties are readily apparent (Table S1). For example, the highest Young's modulus value of 280 \pm 20 MPa was measured for the shortest dithiol sample (2DT-DAT) and then monotonically decreased to a plateau value of about 100 MPa for x > 4 (Figure 4B).

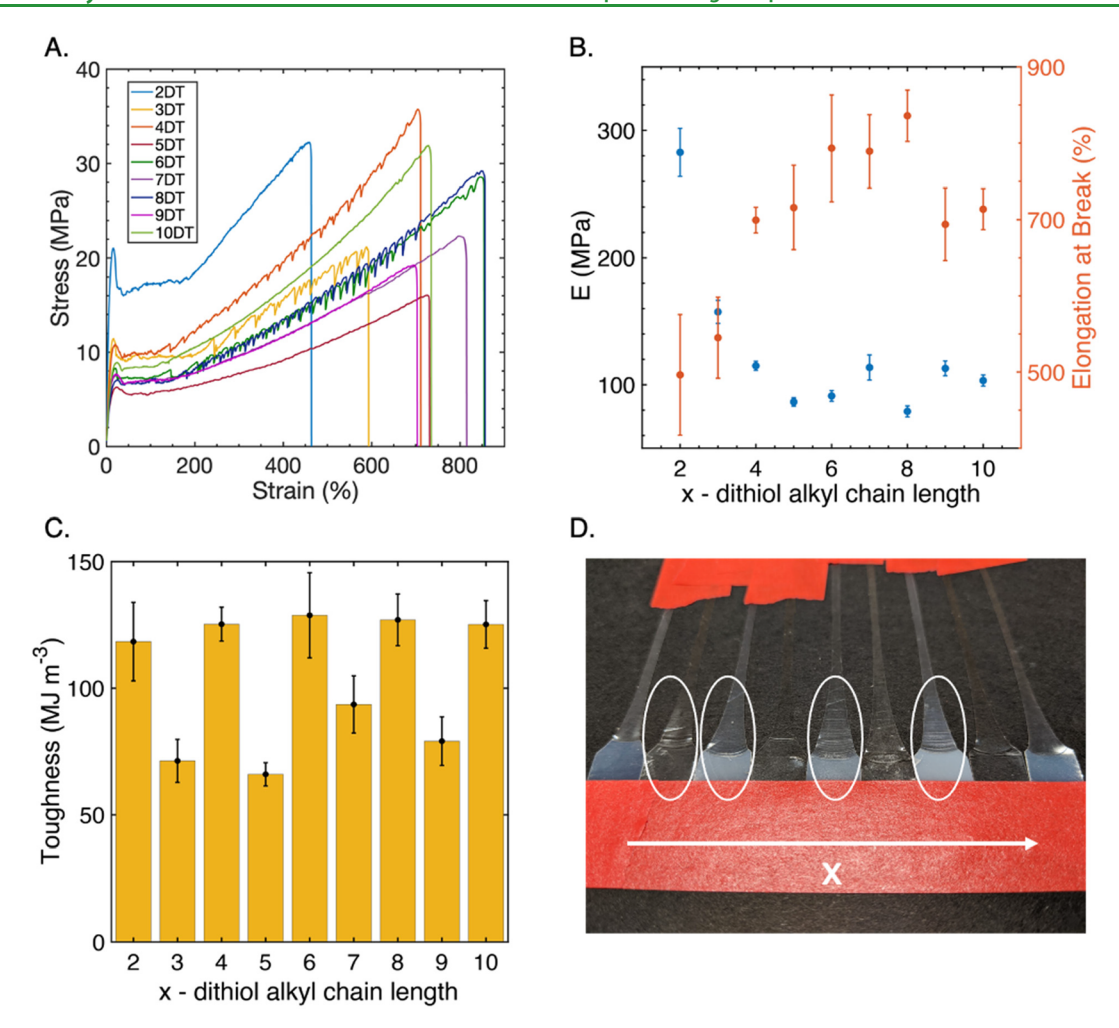


Figure 4. Mechanical characterization of thiol—ene thermoplastic systems. (A) Representative stress—strain tensile plots for the xDT-DAT photopolymers. The thermoplastics with x=3, 4, 6, and 8 show stress oscillations in the strain hardening regime for thermoplastics. (B) Young's modulus (E) and elongation at break (ϵ_{\max}) show a strong dependence on the alkyl dithiol chain length, where E was highest for shorter alkyl chains and ϵ_{\max} increased with chain length until n=8. (C) An apparent odd—even effect on toughness is observed for the thermoplastics. (D) Alternating transparent/opaque bands are observed perpendicular to the tensile direction for samples with stress oscillations.

This factor of 3 difference in E is perhaps due to the relative rigidity of the short alkyl chains combined with the unique conformational packing to yield a stiffer material. The inverse trend was observed for elongation to break where the strain at break increased with alkyl chain length up to 8DT-DAT. Curiously, an apparent dependence on the planarity of the alkyl chain (odd-even effect) was observed for toughness (Figure 4C). The toughness of the even samples was approximately 30-90% greater than the corresponding odd samples because of the enhanced intermolecular interactions of the extended planar chains that ultimately facilitated higher degrees of strain hardening. During strain hardening, certain xDT-DAT thermoplastics exhibited unusual oscillatory dips in the tensile stress that coincided with periodic transparent and opaque banding perpendicular to the direction of strain (Figure 4A,D). Observations of this phenomenon are fairly rare but have been sporadically reported for a number of commercial thermoplastic polymers, including PET, 47-52 HDPE, 53,54 polycarbonate, 55 syndiotactic PP, 50,53,56,57 copolyesters, 58 polyamide, 53 poly(butylene succinate), 59 and recently synthesized isotactic poly(propylene oxide). 60 These stress oscillations were found to coincide with crazing and the subsequent formation of microcavities within the opaque

bands, ^{59,61} although the source of the oscillations remains unclear. ⁴⁹ The xDT-DAT samples that exhibited these stress oscillations (i.e., 3DT-DAT, 4DT-DAT, 6DT-DAT, and 8DT-DAT) predominately consisted of thermoplastics with multiple melting endotherms and broad $T_{\rm m}$. This behavior is likely due to the large population of smaller, imperfect crystallites at lower $T_{\rm m}$ that are susceptible to crazing. To determine whether the homogenization of crystallite species would diminish or remove stress oscillations, 6DT-DAT was melted above its $T_{\rm m,max}$ and recrystallized at 70 °C over several days prior to rapid quenching. Indeed, tensile testing of the thermally conditioned 6DT-DAT yielded plastic deformation without stress oscillations during strain hardening (Figure S5), confirming that smaller crystallites readily initiate crazing.

Thiol—ene thermoplastics were photopolymerized with structurally similar monomers to simplify comparisons between crystallization and final material properties. However, a multitude of dithiol and dialkene combinations exist that may yield material properties suitable for a diverse set of applications. Therefore, a brief, preliminary investigation of alternative thiol—ene thermoplastics was performed both to determine whether this facile photopolymerization was applicable for other monomers and to further expand the

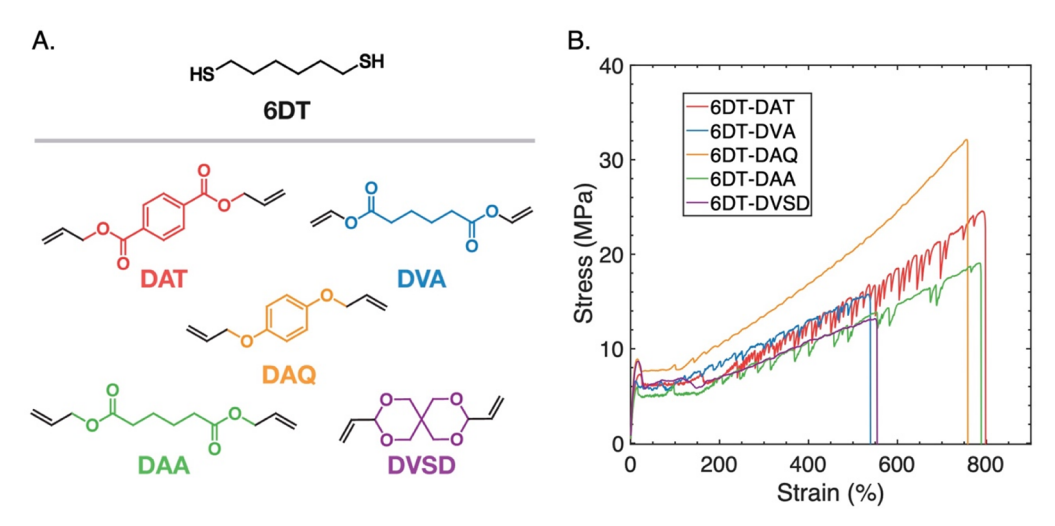


Figure 5. Mechanical characterization of additional thiol—ene thermoplastic systems. (A) Molecular structure of alternative dienes explored as potential photopolymerizable thermoplastics, holding the dithiol (6DT) constant. (B) Representative stress—strain plots of semicrystalline thermoplastics. As with the *x*DT-DAT thiol—enes, slight modifications to the monomer structure yielded critical variations in mechanical performance.

accessible material properties space. Interestingly, high molecular weight $(\sim 10^4~{\rm g~mol}^{-1})$, semicrystalline thermoplastics with mechanical properties markedly similar to 6DT-DAT were obtained by holding 6DT constant and substituting the rigid DAT benzene ring with flexible aliphatic vinyl (divinyl adipate, DVA) and allyl esters (diallyl adipate, DAA) and holding 6DT constant (Figure 5). Mechanical properties comparable to 6DT-DAT were also obtained upon exchanging the benzene ring for a rigid spiroacetal alkene (3,9-divinylspirobi(m-dioxane), DVSD), thus removing the ether/ester functionalities. Our results for the 6DT-DVSD system conflict with previous findings whereby reasonable mechanical performance was only achieved after the addition of a trithiol cross-linker.²¹ Furthermore, replacing the DAT diallyl esters with diallyl ethers (diallyl quinone, DAQ) also led to high molecular weight, semicrystalline materials with Young's modulus and toughness values superior to 6DT-DAT. As with 6DT-DAT, stress oscillations were observed during strain hardening for all of the alternate dienes explored here (although the depth of the oscillations was considerably shallower for 6DT-DAQ and 6DT-DVSD). While the source of this unusual mechanical phenomenon remains unclear, investigation into the molecular structures and processing conditions that give rise to this nonlinear mechanical behavior and reproducible physical striations merits additional future consideration. This cursory investigation into additional varied thiol-ene monomer combinations demonstrates the broad applicability of this simple polymerization technique to obtain thermoplastics with widely variable material properties.

Commercial thermoplastics are highly advantageous because of both their ease of manufacture and potential recyclability after service. Photopolymerizable thermoplastics can vastly expand the range of attainable thermoplastic properties, offering the ability to readily achieve intricate components by using fabrication techniques such as additive manufacturing. Uniquely, the thiol—ene "click" chemistry provides a facile yet robust method for obtaining thermoplastic materials ("click thermoplastics") without requiring high-purity monomers and/or precise stoichiometry to achieve superior mechanical performance. This work provides an initial framework for exploring dithiol and diene combinations with deliberate

structural variations to obtain a diverse array of material properties. Additional modifications to this system beyond simple monomer substitutions may also offer material improvements. One such approach would entail preoligomerization to further control crystallization while simultaneously minimizing the odor that limits the use of thiol—ene chemistries for many commercial applications. Furthermore, the implementation of dithiol or diene mixtures beyond the simple 1:1 system used here may be used as a mechanism to alter crystallinity and material properties, such as obtaining distinct $T_{\rm m}$ s or regions with distinct material domains. 63

CONCLUSIONS

In summary, high molecular weight, semicrystalline thermoplastics were readily obtained via the rapid thiol-ene "click" reaction. Photopolymerization predominantly occurred between commercially available, unpurified dithiols and dienes without controlling for precise stoichiometry. A thorough structure-property investigation into the relationship between monomeric structure, extent and rate of crystallization, and final material properties was conducted by varying the alkyl chain length of the dithiol. While seemingly understated, perturbations to both the conformation and length of the alkyl chain drastically impacted the morphology of polymer crystallinity, ultimately altering the optical, thermal, and mechanical behavior of the thermoplastics. To confirm the universal applicability of this photopolymerization method for other thiol-ene systems, alternate diene monomers with widely variable structures were also studied. As with the xDT-DAT thermoplastics, the impressive, though variable, mechanical properties obtained were highly dependent on the substituents present and conformation of the monomer. While the photopolymers examined herein constitute only a small fraction of the potentially advantageous thiol-ene combinations, they serve as a foundation for the tunable development of photopolymerizable thermoplastics with material properties to meet various applications.

ASSOCIATED CONTENT

Supporting Information

The Supporting Information is available free of charge at https://pubs.acs.org/doi/10.1021/acsapm.0c01393.

Real-time FTIR plots, UV—vis transmission spectra, $T_{\rm g}$ and tan delta from DMA, modulus development measured with real-time photorheology, $M_{\rm n}$ of α DT-DAT thiol—ene thermoplastics, summary of mechanical properties, stress—strain plot of thermally treated 6DT-DAT, and NMR spectra of synthesized molecules (PDF)

AUTHOR INFORMATION

Corresponding Author

Jeffrey W. Stansbury — Department of Chemical and Biological Engineering and Materials Science and Engineering Program, University of Colorado Boulder, Boulder, Colorado 80309, United States; Department of Craniofacial Biology, School of Dental Medicine, University of Colorado Denver, Aurora, Colorado 80045, United States; orcid.org/0000-0003-1880-005X; Email: jeffrey.stansbury@cuanschutz.edu

Authors

Kimberly K. Childress — Department of Chemical and Biological Engineering, University of Colorado Boulder, Boulder, Colorado 80309, United States; orcid.org/0000-0001-8525-5712

Marvin D. Alim — Materials Science and Engineering Program, University of Colorado Boulder, Boulder, Colorado 80309, United States; oocid.org/0000-0001-9983-3720

Sudheendran Mavila — Department of Chemical and Biological Engineering, University of Colorado Boulder, Boulder, Colorado 80309, United States

Vikina Martinez – Materials Science and Engineering Program, University of Colorado Boulder, Boulder, Colorado 80309, United States

Yifu Ding — Department of Mechanical Engineering, University of Colorado Boulder, Boulder, Colorado 80309, United States; orcid.org/0000-0001-7779-7781

Christopher N. Bowman — Department of Chemical and Biological Engineering, Materials Science and Engineering Program, and BioFrontiers Institute, University of Colorado Boulder, Boulder, Colorado 80309, United States;
orcid.org/0000-0001-8458-7723

Complete contact information is available at: https://pubs.acs.org/10.1021/acsapm.0c01393

Notes

The authors declare the following competing financial interest(s): A provisional patent on this work has been filed by the Venture Partners at University of Colorado Boulder.

ACKNOWLEDGMENTS

This work was supported by NIH/NIDCR R21DE028444 and NSF DMR 1809841. Imaging work was performed at the BioFrontiers Institute Advanced Light Microscopy Core. A Nikon Ti-E microscope was used to perform super-resolution microscopy and is supported by the Howard Hughes Medical Institute. The Microscopy Core was also used to conduct data analysis and visualization work. The Analysis Workstation was supported by NIH 1S10RR026680-01A1. Furthermore, the

authors thank Prof. Noel Clark, Prof. Joseph MacLennan, and Dr. Mingtao Chen for their helpful discussions and insights.

REFERENCES

- (1) Corrigan, N.; Yeow, J.; Judzewitsch, P.; Xu, J.; Boyer, C. Seeing the Light: Advancing Materials Chemistry through Photopolymerization. *Angew. Chem., Int. Ed.* **2019**, *58* (16), 5170–5189.
- (2) Podgórski, M.; Fairbanks, B. D.; Kirkpatrick, B. E.; Mcbride, M.; Martinez, A.; Dobson, A.; Bongiardina, N. J.; Bowman, C. N. Toward Stimuli-Responsive Dynamic Thermosets through Continuous Development and Improvements in Covalent Adaptable Networks (CANs). *Adv. Mater.* **2020**, 32, 1906876.
- (3) McBride, M. K.; Worrell, B. T.; Brown, T.; Cox, L. M.; Sowan, N.; Wang, C.; Podgorski, M.; Martinez, A. M.; Bowman, C. N. Enabling Applications of Covalent Adaptable Networks. *Annu. Rev. Chem. Biomol. Eng.* **2019**, *10* (1), 175–198.
- (4) Chakma, P.; Konkolewicz, D. Dynamic Covalent Bonds in Polymeric Materials. *Angew. Chem., Int. Ed.* **2019**, 58 (29), 9682–9695
- (5) Deng, S.; Wu, J.; Dickey, M. D.; Zhao, Q.; Xie, T. Rapid Open-Air Digital Light 3D Printing of Thermoplastic Polymer. *Adv. Mater.* **2019**, *31* (39), 1903970.
- (6) Ligon, S. C.; Husár, B.; Wutzel, H.; Holman, R.; Liska, R. Strategies to Reduce Oxygen Inhibition in Photoinduced Polymerization. *Chem. Rev.* **2014**, *114*, 557–589.
- (7) Schoerpf, S.; Catel, Y.; Moszner, N.; Gorsche, C.; Liska, R. Enhanced Reduction of Polymerization-Induced Shrinkage Stress: Via Combination of Radical Ring Opening and Addition Fragmentation Chain Transfer. *Polym. Chem.* **2019**, *10* (11), 1357–1366.
- (8) Marvel, C. S.; Chambers, R. R. Polyalkylene Sulfides from Diolefins and Dimercaptans. *J. Am. Chem. Soc.* **1948**, 70 (3), 993–998.
- (9) Jasinski, F.; Rannée, A.; Schweitzer, J.; Fischer, D.; Lobry, E.; Croutxé-Barghorn, C.; Schmutz, M.; Le Nouen, D.; Criqui, A.; Chemtob, A. Thiol-Ene Linear Step-Growth Photopolymerization in Miniemulsion: Fast Rates, Redox-Responsive Particles, and Semicrystalline Films. *Macromolecules* **2016**, 49 (4), 1143–1153.
- (10) Xu, J.; Boyer, C. Visible Light Photocatalytic Thiol-Ene Reaction: An Elegant Approach for Fast Polymer Postfunctionalization and Step-Growth Polymerization. *Macromolecules* **2015**, 48 (3), 520–529.
- (11) Sarapas, J. M.; Tew, G. N. Poly(Ether-Thioethers) by Thiol-Ene Click and Their Oxidized Analogues as Lithium Polymer Electrolytes. *Macromolecules* **2016**, 49 (4), 1154–1162.
- (12) Sarapas, J. M.; Tew, G. N. Thiol-Ene Step-Growth as a Versatile Route to Functional Polymers. *Angew. Chem., Int. Ed.* **2016**, 55 (51), 15860–15863.
- (13) Kwasny, M. T.; Watkins, C. M.; Posey, N. D.; Matta, M. E.; Tew, G. N. Functional Polyethylenes with Precisely Placed Thioethers and Sulfoniums through Thiol-Ene Polymerization. *Macromolecules* **2018**, *51* (11), 4280–4289.
- (14) Porel, M.; Alabi, C. A. Sequence-Defined Polymers via Orthogonal Allyl Acrylamide Building Blocks. *J. Am. Chem. Soc.* **2014**, *136* (38), 13162–13165.
- (15) Harguindey, A.; Domaille, D. W.; Fairbanks, B. D.; Wagner, J.; Bowman, C. N.; Cha, J. N. Synthesis and Assembly of Click-Nucleic-Acid-Containing PEG-PLGA Nanoparticles for DNA Delivery. *Adv. Mater.* **2017**, 29 (24), 1700743.
- (16) Xi, W.; Pattanayak, S.; Wang, C.; Fairbanks, B.; Gong, T.; Wagner, J.; Kloxin, C. J.; Bowman, C. N. Clickable Nucleic Acids: Sequence-Controlled Periodic Copolymer/Oligomer Synthesis by Orthogonal Thiol-X Reactions. *Angew. Chem., Int. Ed.* **2015**, *54* (48), 14462–14467.
- (17) Liu, Z.; Fairbanks, B.; He, L.; Liu, T.; Shah, P.; Cha, J. N.; Stansbury, J. W.; Bowman, C. N. Water-Soluble Clickable Nucleic Acid (CNA) Polymer Synthesis by Functionalizing the Pendant Hydroxyl. *Chem. Commun.* **2017**, *53* (73), 10156–10159.
- (18) Han, X.; Domaille, D. W.; Fairbanks, B. D.; He, L.; Culver, H. R.; Zhang, X.; Cha, J. N.; Bowman, C. N. New Generation of

- Clickable Nucleic Acids: Synthesis and Active Hybridization with DNA. *Biomacromolecules* **2018**, *19* (10), 4139–4146.
- (19) Jin, K.; Leitsch, E. K.; Chen, X.; Heath, W. H.; Torkelson, J. M. Segmented Thermoplastic Polymers Synthesized by Thiol-Ene Click Chemistry: Examples of Thiol-Norbornene and Thiol-Maleimide Click Reactions. *Macromolecules* **2018**, *51* (10), 3620–3631.
- (20) Alim, M. D.; Childress, K. K.; Baugh, N. J.; Martinez, A. M.; Davenport, A.; Fairbanks, B. D.; Mcbride, M. K.; Worrell, B. T.; Stansbury, J. W.; Mcleod, R.; Bowman, C. N. A Photopolymerizable Thermoplastic with Tunable Mechanical Performance. *Mater. Horiz.* **2020**, *7*, 835–842.
- (21) Sycks, D. G.; Safranski, D. L.; Reddy, N. B.; Sun, E.; Gall, K. Tough Semicrystalline Thiol—Ene Photopolymers Incorporating Spiroacetal Alkenes. *Macromolecules* **2017**, *50* (11), 4281–4291.
- (22) Shi, S.; Pan, Y.; Lu, B.; Zheng, G.; Liu, C.; Dai, K.; Shen, C. Realizing the Simultaneously Improved Toughness and Strength of Ultra-Thin LLDPE Parts through Annealing. *Polymer* **2013**, *54* (25), 6843–6852.
- (23) Bas, C.; Battesti, P.; Albérola, N. D. Crystallization and Melting Behaviors of Poly(Aryletheretherketone) (PEEK) on Origin of Double Melting Peaks. *J. Appl. Polym. Sci.* **1994**, *53* (13), 1745–1757.
- (24) Bassett, D. C.; Olley, R. H.; Al Raheil, I. A. M. On Crystallization Phenomena in PEEK. *Polymer* **1988**, 29 (10), 1745–1754.
- (25) Lattimer, M. P.; Hobbs, J. K.; Hill, M. J.; Barham, P. J. On the Origin of the Multiple Endotherms in PEEK. *Polymer* **1992**, *33* (18), 3971–3973.
- (26) Mai, K.; Wang, K.; Zeng, H. Multiple Melting Behavior of Nucleated Polypropylene. J. Appl. Polym. Sci. 2003, 88 (6), 1608–1611
- (27) Shan, G. F.; Yang, W.; Tang, X. G.; Yang, M. B.; Xie, B. H.; Fu, Q.; Mai, Y. W. Multiple Melting Behaviour of Annealed Crystalline Polymers. *Polym. Test.* **2010**, 29 (2), 273–280.
- (28) Serrano, P. J M.; Thuss, E.; Gaymans, R. J. Alternating Polyesteramides Based on 1,4-Butylene Terephthalamide: 2. Alternating Polyesteramides Based on a Single, Linear Diol (4NTm). *Polymer* **1997**, 38 (15), 3893–3902.
- (29) Kricheldorf, H. R.; Schwarz, G.; de Abajo, J.; de la Campa, J. G. LC-Polyimides: 5. Poly(Ester-Imide)s Derived from N-(4-Carboxyphenyl) Trimellitimide and a,w-Dihydroxylalkanes. *Polymer* **1991**, 32 (5), 942–949.
- (30) Mishra, M. K.; Varughese, S.; Ramamurty, U.; Desiraju, G. R. Odd-Even Effect in the Elastic Modulii of α,ω Alkanedicarboxylic Acids. *J. Am. Chem. Soc.* **2013**, *135* (22), 8121–8124.
- (31) Thalladi, V. R.; Nüsse, M.; Boese, R. The Melting Point Alternation in α,ω -Alkanedicarboxylic Acids. *J. Am. Chem. Soc.* **2000**, 122 (38), 9227–9236.
- (32) Liau, W. B.; Boyd, R. H. Structure and Packing in Crystalline Aliphatic Polyesters. *Macromolecules* **1990**, 23 (5), 1531–1539.
- (33) Zhou, C.; Wei, Z.; Yu, Y.; Shao, S.; Leng, X.; Wang, Y.; Li, Y. Biobased Long-Chain Aliphatic Polyesters of 1,12-Dodecanedioic Acid with a Variety of Diols: Odd-Even Effect and Mechanical Properties. *Mater. Today Commun.* 2019, 19 (March), 450–458.
- (34) Bikiaris, D. N.; Papageorgiou, G. Z.; Giliopoulos, D. J.; Stergiou, C. A. Correlation between Chemical and Solid-State Structures and Enzymatic Hydrolysis in Novel Biodegradable Polyesters. The Case of Poly(Propylene Alkanedicarboxylate)S. *Macromol. Biosci.* **2008**, 8 (8), 728–740.
- (35) Lu, J.; Wu, L.; Li, B. G. High Molecular Weight Polyesters Derived from Biobased 1,5-Pentanediol and a Variety of Aliphatic Diacids: Synthesis, Characterization, and Thermomechanical Properties. ACS Sustainable Chem. Eng. 2017, 5 (7), 6159–6166.
- (36) Craig, A. A.; Imrie, C. T. Effect of Backbone Flexibility on the Thermal Properties of Side-Group Liquid-Crystal Polymers. *Macromolecules* 1999, 32 (19), 6215–6220.
- (37) Francisca Mary, L. J.; Kannan, P. Studies on Odd-Even Effect of Methylene Spacers in Poly(Pyromellitimide-Urethane)S. *J. Macromol. Sci., Part A: Pure Appl.Chem.* **1999**, *36* (9), 1289–1305.

- (38) Sirrine, J. M.; Meenakshisundaram, V.; Moon, N. G.; Scott, P. J.; Mondschein, R. J.; Weiseman, T. F.; Williams, C. B.; Long, T. E. Functional Siloxanes with Photo-Activated, Simultaneous Chain Extension and Crosslinking for Lithography-Based 3D Printing. *Polymer* **2018**, *152*, 25–34.
- (39) Andjelic, S.; Scogna, R. C. Polymer Crystallization Rate Challenges: The Art of Chemistry and Processing. *J. Appl. Polym. Sci.* **2015**, *1*32 (38), 1–15.
- (40) Pan, P.; Liang, Z.; Cao, A.; Inoue, Y. Layered Metal Phosphonate Reinforced Poly(L-Lactide) Composites with a Highly Enhanced Crystallization Rate. ACS Appl. Mater. Interfaces 2009, 1 (2), 402–411.
- (41) Li, L.; Li, B.; Hood, M. A.; Li, C. Y. Carbon Nanotube Induced Polymer Crystallization: The Formation of Nanohybrid Shish-Kebabs. *Polymer* **2009**, *50*, 953–965.
- (42) Mercier, J. P. Nucleation in Polymer Crystallization: A Physical or a Chemical Mechanism? *Polym. Eng. Sci.* **1990**, *30* (5), 270–278.
- (43) Napolitano, S.; Wübbenhorst, M. Slowing down of the Crystallization Kinetics in Ultrathin Polymer Films: A Size or an Interface Effect? *Macromolecules* **2006**, *39* (18), 5967–5970.
- (44) Nunes, R. W.; Martin, J. R.; Johnson, J. F. Influence of Molecular Weight and Molecular Weight Distribution on Mechanical Properties of Polymers. *Polym. Eng. Sci.* **1982**, 22 (4), 205–228.
- (45) Konstandakopoulou, F. D.; Gravalos, K. G.; Kallitsis, J. K. Synthesis and Characterization of Processable Aromatic-Aliphatic Polyethers with Quinquephenyl Segments in the Main Chain for Light-Emitting Applications. *Macromolecules* **1998**, *31* (16), 5264–5271.
- (46) Jabbari-Farouji, S.; Rottler, J.; Lame, O.; Makke, A.; Perez, M.; Barrat, J. L. Plastic Deformation Mechanisms of Semicrystalline and Amorphous Polymers. *ACS Macro Lett.* **2015**, *4* (2), 147–150.
- (47) Andrianova, G. P.; Kechekyan, A. S.; Kargin, V. A. Self-Oscillation Mechanism of Necking on Extension of Polymers. *J. Polym. Sci. Part A-2* **1971**, *9*, 1919–1933.
- (48) Pakula, T.; Fischer, E. W. Instabilities of the Deformation Process in Cold Drawing of Poly(Ethylene Terephthalate) and Other Polymers. J. Polym. Sci., Polym. Phys. Ed. 1981, 19 (11), 1705–1726.
- (49) Ronkay, F.; Czigány, T. Cavity Formation and Stress-Oscillation during the Tensile Test of Injection Molded Specimens Made of PET. *Polym. Bull.* **2006**, *57* (6), 989–998.
- (50) Ebener, H.; Pleuger, B.; Petermann, J. Stress and Strain Oscillations in Syndiotactic Polypropylene and in Poly-(Ethyleneterephthalate). *J. Appl. Polym. Sci.* **1999**, *71* (5), 813–817.
- (51) Toda, A. Oscillation and Instability of Neck Propagation in Poly(Ethylene Terephthalate) Films. *Polymer* **1993**, *34* (11), 2306–2314
- (52) Toda, A.; Tomita, C.; Hikosaka, M.; Hibino, Y.; Miyaji, H.; Nonomura, C.; Suzuki, T.; Ishihara, H. Thermomechanical Coupling and Self-Excited Oscillation in the Neck Propagation of PET Films. *Polymer* **2002**, 43 (3), 947–951.
- (53) Bazhenov, S. L.; Rodionova, Y. A.; Kechek'yan, A. S. Self-Oscillation Neck Propagation in Various Polymers. *Polym. Sci., Ser. A* **2003**, *45* (7), 635–639.
- (54) Mouzakis, D. E.; Karger-Kocsis, J. Effects of Gasoline Absorption on the Tensile Impact Response of HDPE/Selar Laminar Microlayer Composites. *J. Appl. Polym. Sci.* **1998**, *68* (4), 561–569.
- (55) Chiang, D.; Tsai, M.-L.; Lee, S. The Tensile Force Oscillation of Polycarbonate at Elevated Temperatures. *Polym. Eng. Sci.* **2013**, *53*, 589–596
- (56) Karger-Kocsis, J.; Shang, P. P. A Modulated DSC Study on the Stress Oscillation Phenomenon in a Syndiotactic Polypropylene. *J. Therm. Anal. Calorim.* **2002**, *69* (2), 499–507.
- (57) García Gutiérrez, M. C.; Karger-Kocsis, J.; Riekel, C. Stress Oscillation-Induced Modulated Phase Transformation and Yielding in Syndiotactic Polypropylene. *Chem. Phys. Lett.* **2004**, 398 (1–3), 6–10.
- (58) Karger-Kocsis, J.; Czigány, T.; Moskala, E. J. Stress Oscillation in Amorphous Copolyesters Due to Tensile Impact. *Polym. Eng. Sci.* **1999**, 39 (8), 1404–1411.

- (59) Wan, C.; Heeley, E. L.; Zhou, Y.; Wang, S.; Cafolla, C. T.; Crabb, E. M.; Hughes, D. J. Stress-Oscillation Behaviour of Semi-Crystalline Polymers: The Case of Poly(Butylene Succinate). *Soft Matter* **2018**, *14* (45), 9175–9184.
- (60) Lipinski, B. M.; Morris, L. S.; Silberstein, M. N.; Coates, G. W. Isotactic Poly(Propylene Oxide): A Photodegradable Polymer with Strain Hardening Properties. *J. Am. Chem. Soc.* **2020**, *142* (14), 6800–6806.
- (61) Wan, T.; Zhang, J.; Liao, S.; Du, T. An Investigation of Stress Oscillation in Poly(Butylene Succinate-Co-Cyclohexanedimethylene Succinate). *Polym. Eng. Sci.* **2015**, *55*, 966–974.
- (62) Mondal, M. K.; Bose, B. P.; Bansal, P. Recycling Waste Thermoplastic for Energy Efficient Construction Materials: An Experimental Investigation. *J. Environ. Manage.* **2019**, 240, 119–125.
- (63) Song, H.; Fang, Z.; Jin, B.; Pan, P.; Zhao, Q.; Xie, T. Synergetic Chemical and Physical Programming for Reversible Shape Memory Effect in a Dynamic Covalent Network with Two Crystalline Phases. ACS Macro Lett. 2019, 8 (6), 682–686.